

**Fig. 5.** Selective activation of TAB1-dependent and TAB1-independent p38 $\alpha$  activation pathways. (A) Requirement of intrinsic p38 $\alpha$  activity for p38 $\alpha$  phosphorylation induced by extracellular stimuli. The HEK 293 cells, pretreated with or without SB203580 (5  $\mu$ M) for 30 min, were stimulated with TNF (100 ng/ml), peroxyntirite (500  $\mu$ M), anisomycin (50 ng/ml), or sorbitol (0.4 M) for 30, 5, 30, and 30 min, respectively. Amounts of p38 $\alpha$  and phospho-p38 $\alpha$  were determined by immunoblotting with antibodies against flag and phospho-p38. (B) Effect of SB203580 on p38 $\alpha$  phosphorylation in RPMI 8226 cells. Cells were stimulated with CpG oligonucleotide (5  $\mu$ g/ml), LPS (100 ng/ml), or lipoprotein (lipo) (200 ng/ml) for 30 min. Amounts of phospho-p38 $\alpha$  and p38 $\alpha$  were determined by immunoblotting. (C) Distinct signaling to p38 $\alpha$  by TLR2 and TLR4. Flag-p38 $\alpha$ , flag-p38 $\alpha$ (M), or flag-p38 $\alpha$ (DA) was expressed in HEK 293 cells with or without TLR2 or TLR4, and with or without TAB1( $\Delta$ 313-418) as indicated. The cells were treated with SB203580 and stimulated with lipoprotein or LPS as indicated. Amounts of p38 $\alpha$  and phospho-p38 $\alpha$  were determined by immunoblotting. (D) Interaction of TRAF6 with TAB1-p38 $\alpha$ . TLR4-293 cells were transfected with expression plasmids encoding Myc-TRAF6, HA-p38 $\alpha$ , and flag-TAB1 in various combinations and exposed to LPS as indicated. Immunoprecipitates with flag-specific antibody and cell lysates were analyzed by immunoblotting with antibodies against Myc, HA, and flag. (E) Proposed signaling pathway upstream of TAB1-mediated p38 $\alpha$  activation. Data shown in (A to D) are representative of two to three independent experiments.

Effect of SB203580 on p38 $\alpha$  phosphorylation in RPMI 8226 cells. Cells were stimulated with CpG oligonucleotide (5  $\mu$ g/ml), LPS (100 ng/ml), or lipoprotein (lipo) (200 ng/ml) for 30 min. Amounts of phospho-p38 $\alpha$  and p38 $\alpha$  were determined by immunoblotting. (C) Distinct signaling to p38 $\alpha$  by TLR2 and TLR4. Flag-p38 $\alpha$ , flag-p38 $\alpha$ (M), or flag-p38 $\alpha$ (DA) was expressed in HEK 293 cells with or without TLR2 or TLR4, and with or without TAB1( $\Delta$ 313-418) as indicated. The cells were treated with SB203580 and stimulated with lipoprotein or LPS as indicated. Amounts of p38 $\alpha$  and phospho-p38 $\alpha$  were determined by immunoblotting. (D) Interaction of TRAF6 with TAB1-p38 $\alpha$ . TLR4-293 cells were transfected with expression plasmids encoding Myc-TRAF6, HA-p38 $\alpha$ , and flag-TAB1 in various combinations and exposed to LPS as indicated. Immunoprecipitates with flag-specific antibody and cell lysates were analyzed by immunoblotting with antibodies against Myc, HA, and flag. (E) Proposed signaling pathway upstream of TAB1-mediated p38 $\alpha$  activation. Data shown in (A to D) are representative of two to three independent experiments.

or together with TRAF6, the complexes were coimmunoprecipitated with TAB1. Stimulation of cells with LPS increased the amount of coprecipitated-TRAF6 and -p38 $\alpha$  (Fig. 5D), suggesting enhanced formation of a TRAF6-TAB1-p38 complex. Thus, the TAB1-p38 $\alpha$  pathway may be directly linked with TRAF6 (Fig. 5E).

Signal transduction is controlled not only by enzymes, but also by nonenzymatic adapters, scaffolds and other "inert" proteins. Much like these adapters, TAB1 binds various kinases such as TAK1 and p38 $\alpha$ . However, a difference between TAB1 and the other nonenzymatic modulators of the MAP kinase pathway is that binding with TAB1 results in kinase activation. Direct mediation of p38 $\alpha$  activation by TAB1 represents a new mechanism of activation distinct from the well-known activation by MAPKK (1-7). Although autophosphorylation of MAP kinase has been observed in vitro, it occurred at such a low level that it was not considered a primary activation mechanism (21-23). The autoactivation of p38 $\alpha$  MAP kinases facilitated by interaction with regulatory molecule(s) could be an important alternative activation pathway operating in parallel with kinase cascades in regulating intracellular signaling.

11. B. Ge, H. Gram, F. Di Padova, J. Han, data not shown.
12. S. Kumar, et al., *Biochem. Biophys. Res. Commun.* **263**, 825 (1999).
13. B. Frantz et al., *Biochemistry* **37**, 13846 (1998).
14. A. Galan et al., *J. Biol. Chem.* **275**, 11418 (2000).
15. S. Zhuang et al., *J. Biol. Chem.* **275**, 25939 (2000).
16. T. Matsuguchi et al., *J. Immunol.* **165**, 5767 (2000).
17. J.-H. Her et al., *Biochem. J.* **296**, 25 (1993).
18. Single-letter abbreviations for the amino acid residues are as follows: A, Ala; C, Cys; D, Asp; E, Glu; F, Phe; G, Gly; H, His; I, Ile; K, Lys; L, Leu; M, Met; N, Asn; P, Pro; Q, Gln; R, Arg; S, Ser; T, Thr; V, Val; W, Trp; and Y, Tyr.
19. J. Imler, J. A. Hoffmann, *Trends Cell Biol.* **11**, 304 (2001).

20. J. Ninomiya-Tsuji et al., *Nature* **398**, 252 (1999).
21. J. Wu et al., *Proc. Natl. Acad. Sci. U.S.A.* **88**, 9508 (1991).
22. D. J. Robbins et al., *J. Biol. Chem.* **268**, 5097 (1993).
23. A. J. Rossomando et al., *Proc. Natl. Acad. Sci. U.S.A.* **89**, 5779 (1992).
24. J. Han et al., *Nature* **386**, 296 (1997).
25. We thank B. Beutler, B. Su, J. E. Ferrell, B. Federici, and U. Knaus for critical reading of the manuscript and J. V. Kuhans for secretarial assistance. Supported by grants from the National Institutes of Health (AI41637 and HL07195).

19 October 2001; accepted 20 December 2001

# Cytoskeletal Regulation by the Nedd8 Ubiquitin-Like Protein Modification Pathway

Thimo Kurz,<sup>1</sup> Lionel Pintard,<sup>2</sup> John H. Willis,<sup>1</sup>  
Danielle R. Hamill,<sup>1\*</sup> Pierre Gönczy,<sup>2</sup> Matthias Peter,<sup>2</sup>  
Bruce Bowerman<sup>1†</sup>

The Nedd8 ubiquitin-like protein modification pathway regulates cell-cycle progression. Our analysis of Nedd8 requirements during *Caenorhabditis elegans* embryogenesis indicates that the cytoskeleton is another target. Nedd8 conjugation negatively regulated contractility of the microfilament-rich cell cortex during pronuclear migration and again during cytokinesis. The Nedd8 pathway also was required after meiosis to negatively regulate katanin, a microtubule-severing complex, permitting the assembly of a large mitotic spindle. We propose that Nedd8-modified cullin, as part of an E3 ubiquitin ligase complex, targets katanin for degradation during the transition from meiosis to mitosis.

Ubiquitin (UBQ) and ubiquitin-like proteins (UBLs) are a family of small, conserved polypeptides that become covalently attached to other proteins. UBQ usually targets proteins for degradation by the proteasome (1, 2), whereas modification by UBLs can affect instead the subcellular localization of target proteins, their

conformation, and their association with other proteins (3). Related pathways mediate the attachment of UBQ and UBLs to targeted proteins (4). In reactions that require ATP, UBQ and UBLs are first covalently attached to cognate E1-activating enzymes and then transferred to E2-conjugating enzymes that, directly

**References and Notes**

1. M. J. Robinson, M. H. Cobb, *Curr. Opin. Cell Biol.* **9**, 180 (1997).
2. K. J. Blumer, G. L. Johnson, *Trends Biochem. Sci.* **19**, 263 (1994).
3. B. Derijard et al., *Science* **267**, 682 (1995).
4. J. Han et al., *J. Biol. Chem.* **271**, 2886 (1996).
5. T. Morguchi et al., *J. Biol. Chem.* **271**, 26981 (1996).
6. J. Ringeaud et al., *Mol. Cell Biol.* **16**, 1247 (1996).
7. A. Cuenda et al., *EMBO J.* **15**, 4156 (1996).
8. Supplementary materials are available on Science Online at [www.sciencemag.org/cgi/content/full/295/5558/1291/DC1](http://www.sciencemag.org/cgi/content/full/295/5558/1291/DC1)
9. H. Shibuya et al., *Science* **272**, 1179 (1996).
10. K. Kishimoto et al., *J. Biol. Chem.* **275**, 7359 (2000).

## REPORTS

or with the help of an E3 ubiquitin ligase, mediate final transfer of UBQ and/or UBLs to target proteins. An E3 ligase has been identified for the UBL SUMO (5), and parts of the SCF ubiquitin-ligase complex may act not only on ubiquitin but also on the UBL called Nedd8 in mammals and Rub1p in the budding yeast *Saccharomyces cerevisiae* (6).

The only known targets of the UBL Nedd8 are cullin proteins. For example, Rub1p modifies the yeast cullin Cdc53p (7). Cdc53p is required for the ubiquitin-mediated degradation of the CDK inhibitor Sic1p in late G<sub>1</sub>, promoting the cell-cycle transition from G<sub>1</sub> to S phase (8, 9). Although Cdc53p is required for viability, Rub1p modification of Cdc53p is not. However, loss-of-function Rub1 mutations are synthetically lethal in combination with temperature-sensitive (ts) alleles of essential E3 ubiquitin ligase subunits, including Cdc53p (7), and Nedd8 conjugation is essential in fission yeast (10). Nedd8-modified cullins are present within SCF (Skp1/cullin-1/F-Box) and CBC (cullin-2/elongin BC) E3 ubiquitin ligase complexes (11), and neddylated cullins can accelerate the recruitment of E-2-bound ubiquitin to the SCF ligase complex (12). The Nedd8 pathway may therefore regulate SCF activity or specify a subset of its targets.

We began our study of Nedd8 requirements in *C. elegans* by identifying a recessive, conditional, maternal effect, embryonic lethal mutation in a gene we call *rfl-1* (13). At restrictive temperatures, homozygous *rfl-1(or198ts)* hermaphrodites produce embryos that fail to hatch (13), referred to hereafter as *rfl-1* mutant embryos or *rfl-1* mutants. Using Nomarski differential interference contrast (DIC) optics [see supplemental material for methods (13)], we made time-lapse recordings of mitosis in *rfl-1* mutants and observed prominent defects in microfilament- and microtubule-mediated processes. Ectopic cleavage furrows formed during cytokinesis, mitotic spindles were misoriented, and nuclei became displaced toward the cell cortex after mitosis (Fig. 1A) (13). Membrane ruffling and furrowing, and nuclear displacement, persisted for several minutes during interphase of the subsequent cell cycle. In 18 out of 33 *rfl-1(or198ts)* mutant embryos, all cleavage furrows regressed (Fig. 1A) (13).

We determined that the locus identified by the *or198ts* mutation corresponds to the predicted gene F11H8.1 (13). BLAST searches indicated that RFL-1/F11H8.1 is the *C. el-*

*egans* member of the Uba3 family of E1-activating enzymes (13). In budding yeast, Uba3p and its partner Ula1p form the heterodimeric E1-activating enzyme for Rub1p. The *C. elegans* homologs of Nedd8, Ubc12, and Ula1 are required for differentiation of the larval epidermis (14), and embryonic requirements for *ubc-12* were described in an RNAi survey of chromosome I loci (15). We observed weakly penetrant lethal effects on embryos when using RNA interference to reduce *rfl-1* function, although the *rfl-1(or198ts)* mutation resulted in fully penetrant embryonic lethality (13). RNAi more fully inactivated other components of the NED-8 pathway, causing penetrant embryonic lethality and an Rfl-1-like phenotype (Fig. 1B). After testing each of the five *C. elegans* cullin genes, we detected Rfl-1-like defects only in *cul-2(RNAi)* and *cul-3(RNAi)* embryos. Depleting *cul-3* resulted in penetrant Rfl-1-like defects (8 out of 9 embryos, see Fig. 1B). Only 2 out of 9 *cul-2(RNAi)* embryos resembled *rfl-1* mutants, whereas severe chromosome segregation and cytokinesis defects, without ectopic furrowing, occurred in 4 out of 9 embryos. Reducing the function of

the ubiquitin-activating enzyme CeUba1 and the SMT3/SUMO-activating enzymes CeUba2 and CeSae2 did not result in Rfl-1-like phenotypes (13).

To confirm that the *or198ts* mutation, and RNAi with other pathway components, reduced NED-8 protein modification, polyclonal antibodies were generated that recognize a NED-8 peptide antigen (13). Using indirect immunofluorescence, we detected NED-8 throughout the cytoplasm of fixed, wild-type embryonic cells during interphase and mitosis, and NED-8 was prominently nuclear during interphase (Fig. 2A). Fluorescence was reduced or eliminated after preincubation with the immunogenic peptide, and little or no signal was detected in fixed *ned-8(RNAi)* mutant embryos (13). In *rfl-1(or198tsRNAi)*, *ula-1(RNAi)*, and *ubc-12(RNAi)* embryos, little or no NED-8 was detected, although NED-8 appeared normal in *cul-3(RNAi)* mutant embryos (Fig. 2B). The staining detected in wild type presumably reflects the distribution of NED-8 targets, with reduction of pathway activity preventing target modification. The normal distribution of NED-8 in *cul-3(RNAi)* mutants is

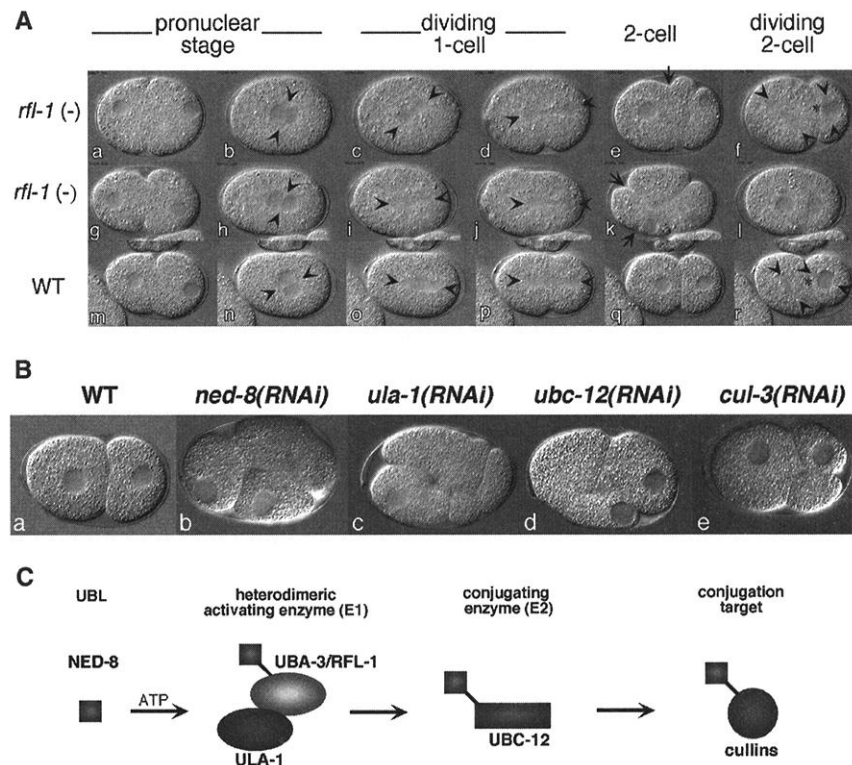


**Fig. 1.** (A) The first two cell divisions in *rfl-1(or198ts)* (a to l) and wild-type (m to r) embryos. Rotation of the first mitotic spindle was often delayed (c, arrowheads), but alignment eventually became normal (d, arrowheads). During cytokinesis, daughter nuclei moved to the cortex (e and k) and ectopic furrows appeared (e and k, arrows). Cytokinesis failed in half the mutants, producing multinucleate one-cell embryos (l). When cytokinesis succeeded, spindle orientation defects occurred in two-cell embryos (f, arrowheads). (B) Mutant embryos from wild-type hermaphrodites microinjected with dsRNA corresponding to *ned-8* (b), *ula-1* (c), *ubc-12* (d), and *cul-3* (e) showed Rfl-1-like defects. Nuclei moved to the cortex and ectopic cleavage furrows appeared. (C) Schematic diagram of the Nedd8 pathway.

<sup>1</sup>Institute of Molecular Biology, University of Oregon, Eugene, OR 97403, USA. <sup>2</sup>Swiss Institute for Experimental Cancer Research (ISREC), CH-1066 Lausanne, Switzerland.

\*Present address: Department of Zoology, Ohio Wesleyan University, Delaware, OH 43015, USA.

†To whom correspondence should be addressed. E-mail: bbowerman@molbio.uoregon.edu

## REPORTS

not surprising, as *cul-2(RNAi)* and *cul-3(RNAi)* mutants exhibit partially distinct but overlapping phenotypes (see above).

As the *or198ts* missense allele may not fully eliminate gene function, we microinjected *rfl-1* double-stranded RNA (dsRNA) into homozygous *rfl-1(or198ts)* hermaphrodites and observed a more severe phenotype. Abnormal membrane ingressions occurred, not only during cytokinesis, but also earlier, when the oocyte and sperm pronuclei were migrating to meet near the posterior pole (Fig. 2C) (13). Before and during pronuclear migration in wild-type embryos, microfilament-dependent membrane contractions occurred anteriorly, accompanied by formation of a prominent membrane ingression called the pseudocleavage furrow. These contractile events occur as the anterior-posterior (a-p) axis is specified, and axis specification

requires microfilaments and myosin motor activity (16, 17). In *rfl-1(or198tsRNAi)* mutant embryos, multiple furrows ingressed deeply during pronuclear migration, although they remained restricted to the anterior (Fig. 2C) (13). Subsequently, pronounced and persistent ectopic furrow ingressions occurred during and after mitosis, and cytokinesis failed in 9 out of 12 *rfl-1(or198tsRNAi)* embryos. These ectopic ingressions in *rfl-1* mutants resembled cleavage furrows, and the contractile ring component CYK-1, normally detected only at the leading edge of the cleavage furrow, accumulated ectopically in *rfl-1* mutants (Fig. 2D). Furthermore, all contractile ring components tested proved to be required for the occurrence of ectopic ingressions in *rfl-1* mutant embryos (Fig. 2E) (13). Reducing the function of central spindle genes, which are required for a late step

in cytokinesis, did not suppress ectopic furrowing (Fig. 2E) (13). To summarize, NED-8 conjugation negatively regulates cortical actomyosin contractility twice, during pronuclear migration and during cytokinesis.

We also observed mitotic spindle positioning defects in *rfl-1(or198ts)* embryos. In wild type, the first mitotic spindle assembled along the a-p axis, after a 90° rotation of the nucleo-centrosomal complex. At the two-cell stage in wild-type embryos, the mitotic spindle in the anterior daughter, AB, remained transversely oriented, whereas the centrosomal axis in the posterior daughter, P<sub>1</sub>, rotated to align with the a-p axis. In *rfl-1(or198ts)* embryos, rotation of the first mitotic spindle was often delayed or incomplete, and the angle of the inter-centrosomal axis relative to the a-p axis over time was more variable (Fig. 3A). In embryos that successfully completed the first division, the P<sub>1</sub> spindle frequently failed to rotate normally (9 out of 18 embryos), and the AB spindle sometimes oriented longitudinally (3 out of 18 embryos).

We next used time-lapse recordings to examine chromosome alignment at metaphase, and chromosome segregation during anaphase (13). Chromosome alignment at metaphase appeared normal, but during anaphase, the two sets of chromosomes separated by only 60% of the wild-type distance (Fig. 3B). We also examined spindle elongation and found that the poles remained close together, achieving only 60% of the wild-type inter-centrosomal distance (Fig. 3D). Thus, reduced chromosome segregation may result from an absence of anaphase B. We also detected lagging chromosomes during anaphase of the first mitosis in 9 out of 28 *rfl-1(or198ts)* mutant embryos, and in *cul-3(RNAi)* embryos (Fig. 3D).

Because astral microtubule contact with the cell cortex influences spindle positioning in *C. elegans* (18–20) and anaphase B in *Drosophila* (21), we examined microtubules using indirect immunofluorescence (13). By metaphase in *rfl-1(or198ts)* embryos ( $n = 18$ ), many astral microtubules failed to reach the cortex, whereas in wild-type embryos ( $n = 10$ ) at metaphase and anaphase, most astral microtubules reached the cortex (Fig. 3C). We also examined spindles in live embryos (Fig. 3E) (13). In wild type, the central spindle remained roughly equidistant between the poles throughout the first embryonic mitosis. In roughly half of the one-cell stage *rfl-1(or198ts)* and *cul-3(RNAi)* mutant embryos examined, the central spindle became displaced toward one or the other pole during anaphase, although it remained centrally positioned in the remainder. Cytokinesis failed in all embryos with displaced central spindles [4 out of 10 *rfl-1(or198ts)* and 5 out of 11 *cul-3(RNAi)* embryos], but was successful if the central spindle remained midway between the poles. Thus the partially penetrant cytokinesis failure in *rfl-1*

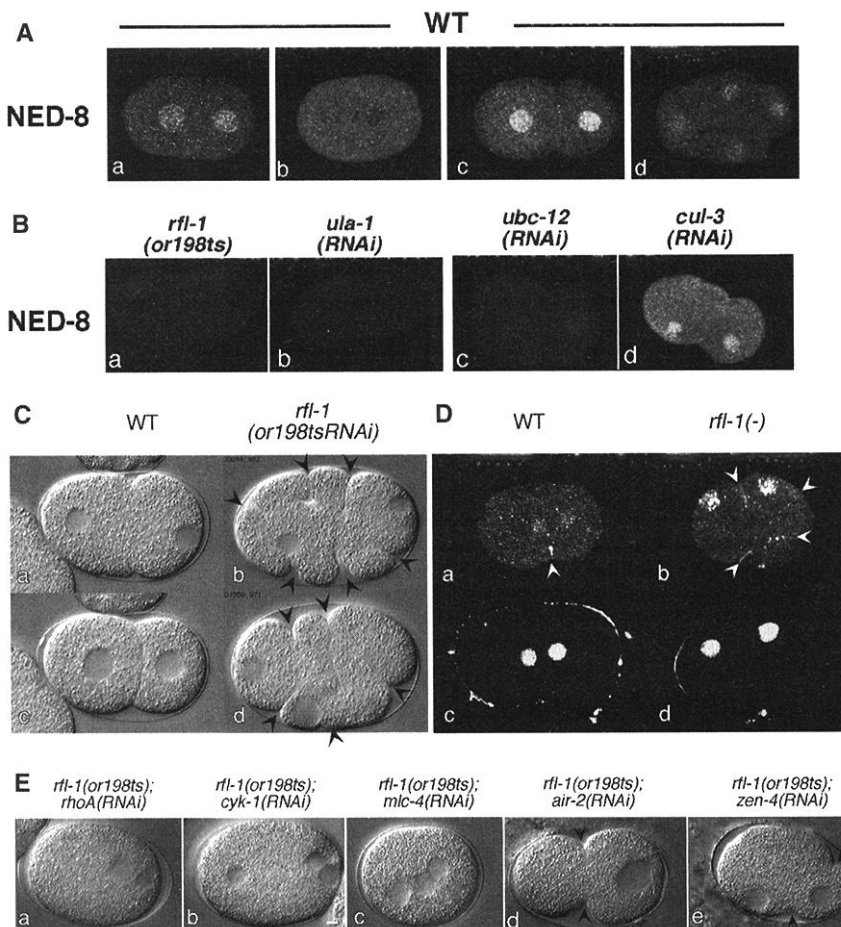


**Fig. 2.** (A) Confocal micrographs show NED-8 protein visualized in fixed embryos by using indirect immunofluorescence. During pronuclear migration (a) and the first mitosis (b), and in 2-cell and 4-cell wild-type embryos during interphase (c and d), NED-8 is cytoplasmic and nuclear. (B) NED-8 levels were reduced at interphase in fixed 2-cell *rfl-1(or198ts)* (a), *ula-1(RNAi)* (b), and *ubc-12(RNAi)* mutant embryos (c) but were unchanged in *cul-3(RNAi)* mutants (d). (C) DIC micrographs of *rfl-1(or198tsRNAi)* embryos with ectopic furrowing (arrowheads) during pronuclear migration (b) and mitosis (d). (D) Confocal micrographs of CYK-1 protein and chromosomal DNA, in fixed embryos shown by indirect immunofluorescence. CYK-1 (arrowheads) localized to the leading edge of cleavage furrows in wild-type embryos (a) and to ectopic furrows in *rfl-1* mutants (b). (E) Nomarski micrographs of embryos from *rfl-1(or198ts)* hermaphrodites micro-injected with dsRNA corresponding to contractile ring genes *rhoA* (a), *cyk-1* (b), and *mlc-4* (c), and central spindle genes *air-2* (d) and *zen-4* (e).

REPORTS

mutants appears to result indirectly from central spindle instability.

Eliminating the function of a *C. elegans* gene called *mel-26* also results in short astral microtubules, spindle orientation defects, and "displaced" pseudocleavage furrows (22, 23). During mitosis, MEL-26 negatively regulates a meiosis-specific katanin encoded by the genes *mei-1* and *mei-2* (24). Mutations in *mei-1* and *mei-2* disrupt meiosis but not mitosis (25, 26). MEI-1 and MEI-2 form a heterodimer, localize to the meiotic spindle and chromosomes, and can destabilize microtubules, consistent with the microtubule-severing activity documented for *Xenopus* katanin. In the absence of *mel-26*, inappropriate MEI-1/2 katanin activity during mitosis results in microtubule instability; loss-of-function mutations in *mei-1* or *mei-2* fully suppress this instability. We therefore examined mitotic spindles in *rfl-1(or198tsRNAi)*; *mei-1(RNAi)* double-mutant embryos and found that reducing *mei-1* function suppressed all signs of microtubule instability (Fig. 4, A and B) (13). Indeed, 10 out of 10 *rfl-1(or198tsRNAi)*; *mei-1(RNAi)* embryos successfully completed cytokinesis, in contrast to the penetrant cytokinesis defect observed in *rfl-1(or198tsRNAi)* mutant embryos (see above). Furthermore, MEI-1 protein localized ectopically to the mitotic spindle and chromosomes in *rfl-1* mutant embryos (Fig. 4C) (13). We therefore suggest that after meiosis the Nedd8 pathway in *C. elegans* targets either MEI-1 or MEI-2 for ubiquitin-mediated degradation, permitting the assembly of a large mitotic spindle.

We isolated the *rfl-1(or198ts)* mutant based on prominent cytoskeletal defects; other studies of the Nedd8 pathway have focused on its role in cell-cycle progression. For example, the mouse *cul-3* gene regulates progression through S phase by targeting cyclin E for ubiquitination (27). Mutations in the *C. elegans* genes *cul-1* and *cul-2* and the yeast cullin *cdc53* affect cell-cycle progression (28–30), and the mammalian ULA1 homolog also is required for transit from S phase to mitosis (31). We therefore examined cell division timing and found that interphase was prolonged in *rfl-1(or198ts)* mutants (Fig. 5A) (13). As early embryonic cells in *C. elegans* alternate between S phase and mitosis with no intervening gap phases (32), the *C. elegans* Nedd8 pathway also appears required for normal progression through S phase.

Having documented a cell-cycle progression defect, we found that reducing *mei-1* function did not suppress the interphase delays (Fig. 5A). Similarly, loss of *mei-1* function did not suppress the ectopic furrowing observed during pronuclear migration in *rfl-1(or198tsRNAi)* embryos (Fig. 4A). Thus the Nedd8 pathway presumably regulates multiple targets. However, ectopic furrowing during mitosis was nearly or entirely suppressed (Fig. 4A). We conclude that during pronuclear migration, negative regulation of cortical contractility is independent of

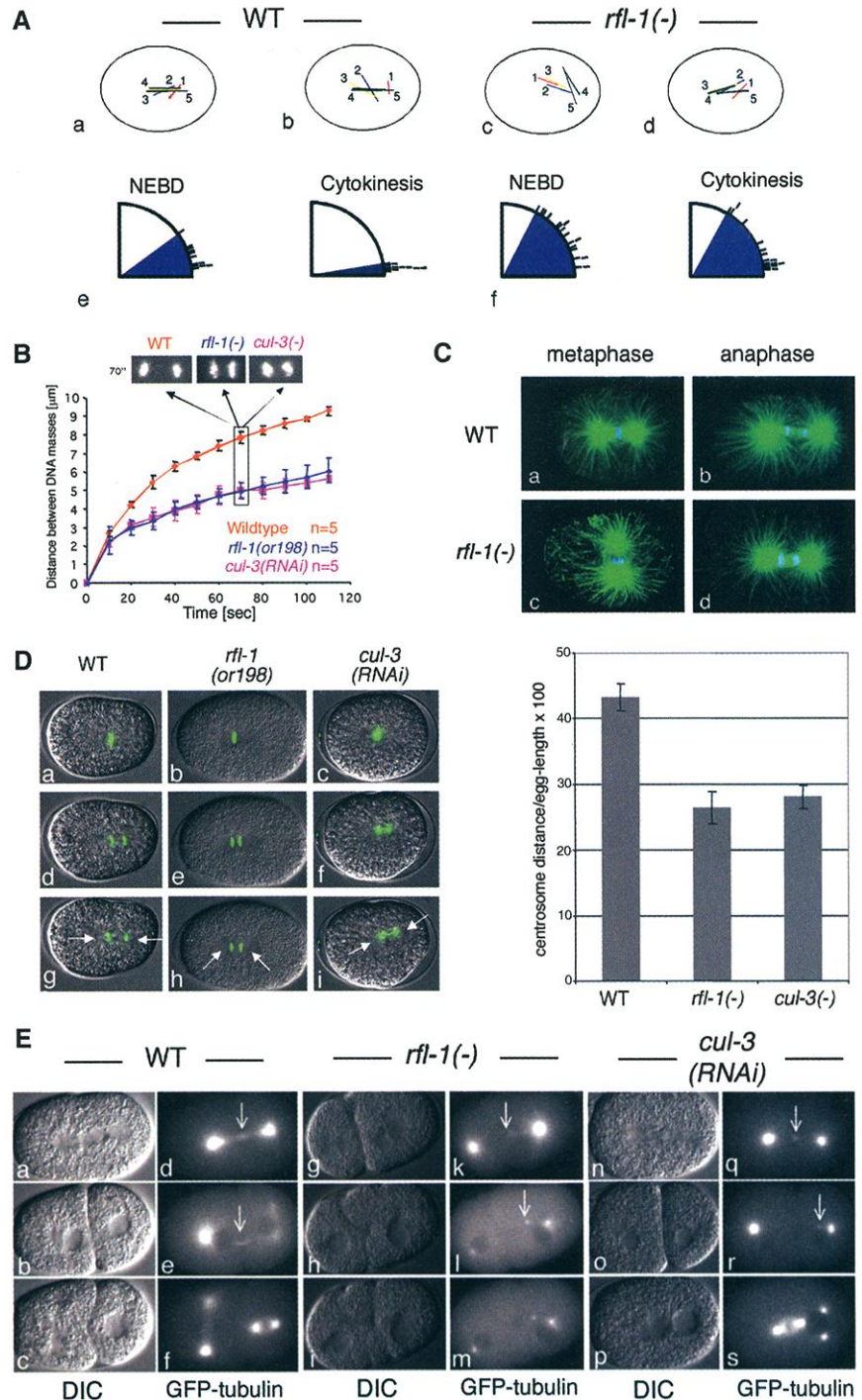


**Fig. 3. (A)** Mitotic spindle orientation in one-cell embryos. In (a to d), mitotic spindle position in individual embryos is depicted at 1-min intervals. Spindle orientation in multiple wild-type (e) and *rfl-1(or198ts)* embryos (f), at nuclear envelope breakdown (NEBD) and during cytokinesis. Alignment along the anterior-posterior axis corresponds to 0 degrees. Each black bar in (e) and (f) represents one embryo. **(B)** Chromosome separation during anaphase, in 10-s intervals, starting at metaphase during the first embryonic mitosis. **(C)** Confocal micrographs of  $\alpha$ -tubulin and DNA in one-cell embryos, fixed for indirect immunofluorescence. In *rfl-1* mutants, many astral microtubules terminated before reaching the cortex (c and d). A spindle orientation defect was apparent at metaphase (c). **(D)** Time-lapse Nomarski and histone::GFP overlays of the first mitosis. Inter-centrosomal distance achieved, relative to total egglength, was plotted for wild-type ( $n = 5$ ), *rfl-1(or198ts)* ( $n = 5$ ), and *cul-3(RNAi)* ( $n = 5$ ) embryos (right). **(E)** Nomarski and tubulin::GFP micrographs of wild-type, *rfl-1(or198ts)* and *cul-3(RNAi)* embryos. The central spindle is visible as bright focus between the centrosomes (arrows).

## REPORTS

microtubules, but that during mitosis, microtubules are required. We therefore used nocodazole as another means of assessing the consequences of destabilizing microtubules (13). During pronuclear migration in nocodazole-treated wild-type embryos, membrane contractions and pseudocleavage furrows were normal, and in nocodazole-treated *rfl-1(or198tsRNAi)* embryos, abnormally active furrowing still occurred (Fig. 5B) (13). However, nocodazole treatment of wild-type embryos during mitosis resulted in a strong Rfl-1-like phenotype, with ectopic and prolonged furrowing, and depletion of the contractile ring component profilin (33) before nocodazole treatment completely suppressed all furrowing (Fig. 5C) (13). Thus disruption of microtubules by nocodazole prevented the negative regulation of cortical microfilament con-

tractility during mitosis, but not during pronuclear migration, consistent with the suppression obtained from *mei-1* loss of function (see above).

Our analysis of microtubule stability and negative regulation of cortical microfilament contractility suggests that the Nedd8 pathway requires an intact spindle to be active during mitosis (13). Consistent with this hypothesis, Skp-1- and Nedd8-modified Cul-1 localize to centrosomes in mammalian tissue culture cells (34), as does the *Drosophila* SCF ubiquitin-ligase component Slimb (35). Thus far, the only known targets of Nedd8 modification are cullins, and neddylated cullins may act only as subunits of SCF ubiquitin-ligases. If so, then NED-8 conjugation may specify a subset of ubiquitin targets, including MEI-1 or MEI-2

after meiosis. It will be interesting to learn whether a Nedd8/katanin regulatory circuit facilitates the transition from meiosis to mitosis in other organisms, and if negative regulation of actomyosin contractility outside the cleavage furrow occurs during cytokinesis in other cell types.

### References and Notes

1. A. Hershko, A. Ciechanover, A. Varshavsky, *Nature Med.* **6**, 1073 (2000).
2. M. Hochstrasser, *Annu. Rev. Genet.* **30**, 405 (1996).
3. S. Jentsch, G. Pyrowolakis, *Trends Cell Biol.* **10**, 335 (2000).
4. M. Hochstrasser, *Science* **289**, 563 (2000).
5. E. S. Johnson, A. A. Gupta, *Cell* **106**, 735 (2001).
6. T. Kamura et al., *Science* **284**, 657 (1999).
7. D. Lammer et al., *Genes Dev.* **12**, 914 (1998).
8. E. Schwob, T. Bohm, M. D. Mendenhall, K. Nasmyth, *Cell* **79**, 233 (1994).
9. C. Bai et al., *Cell* **86**, 263 (1996).
10. F. Osaka et al., *EMBO J.* **19**, 3475 (2000).
11. R. J. Deshaies, *Annu. Rev. Cell Dev. Biol.* **15**, 435 (1999).
12. T. Kawakami et al., *EMBO J.* **20**, 4003 (2001).
13. Supplementary material is available on Science Online at [www.sciencemag.org/cgi/content/full/295/5558/1294/DC1](http://www.sciencemag.org/cgi/content/full/295/5558/1294/DC1)
14. D. Jones, E. P. Candido, *Dev. Biol.* **226**, 152 (2000).
15. P. Zipperlen, A. G. Fraser, R. S. Kamath, M. Martinez-Campos, J. Ahringer, *EMBO J.* **20**, 3984 (2001).
16. S. Guo, K. J. Kemphues, *Nature* **382**, 455 (1996a).
17. C. A. Shelton, J. C. Carter, G. C. Ellis, B. Bowerman, *J. Cell Biol.* **146**, 439 (1999).
18. A. R. Skop, J. G. White, *Curr. Biol.* **8**, 1110 (1998).
19. P. Gonczy et al., *Dev. Cell* **1**, 363 (2001).
20. S. W. Grill, P. Gonczy, E. H. Stelzer, A. A. Hyman, *Nature* **409**, 630 (2001).
21. D. J. Sharp et al., *Mol. Biol. Cell* **11**, 241 (2000).
22. P. E. Mains, K. J. Kemphues, S. A. Sprunger, I. A. Sulston, W. B. Wood, *Genetics* **126**, 593 (1990).
23. M. R. Dow, P. E. Mains, *Genetics* **150**, 119 (1998).
24. M. Srayko, D. W. Buster, O. A. Bazirgan, F. J. McNally, P. E. Mains, *Genes Dev.* **14**, 1072 (2000).
25. S. Clark-Maguire, P. E. Mains, *J. Cell Biol.* **126**, 199 (1994).
26. S. Clark-Maguire, P. E. Mains, *Genetics* **136**, 533 (1994).
27. J. D. Singer, M. Gurian-West, B. Clurman, J. M. Roberts, *Genes Dev.* **13**, 2375 (1999).
28. E. T. Kipreos, L. E. Lander, J. P. Wing, W. W. He, E. M. Hedgecock, *Cell* **85**, 829 (1996).
29. H. Feng et al., *Nature Cell Biol.* **1**, 486 (1999).
30. N. Mathias et al., *Mol. Cell Biol.* **16**, 6634 (1996).
31. Y. Chen, D. L. McPhie, J. Hirschberg, R. L. Neve, *J. Biol. Chem.* **275**, 8929 (2000).
32. L. G. Edgar, J. D. McGhee, *Cell* **53**, 589 (1988).
33. A. Severson, personal communication.
34. E. Freed et al., *Genes Dev.* **13**, 2242 (1999).
35. E. J. Wojcik, D. M. Glover, T. S. Hays, *Curr. Biol.* **10**, 1131 (2000).
36. We thank S. Schneider for phylogenetic analysis of RFL-1; P. Mains, Y. Bobiniec, S. Strome, and A. Severson for providing antibodies; J. Austin and C. Malone for providing GFP lines; Y. Kohara (National Institute of Genetics, Mishima Japan) and E. Kipreos for providing cDNA clones; the *C. elegans* Genetics Center, funded by the NIH National Center for Research Resources, for providing strains; C. Doe, A. Severson and D. Williams for helpful discussions and comments on the manuscript; and V. Hemleben, U. Zentgraf (University of Tübingen, Germany) and U. Brügge (Ludwig-Wilhelm-Gymnasium Rastatt, Germany) for their help and teaching. T.K. was supported by a predoctoral fellowship from the American Heart Association; L.P. by a long-term fellowship from the Federation of European Biochemical Societies; J.H.W. by an NIH Molecular Biology Training Grant; D.R.H. by a postdoctoral fellowship from the American Cancer Society; P.G. and M.P. by the Swiss National Science Foundation; and B.B. was supported by the NIH (R01GM58017).

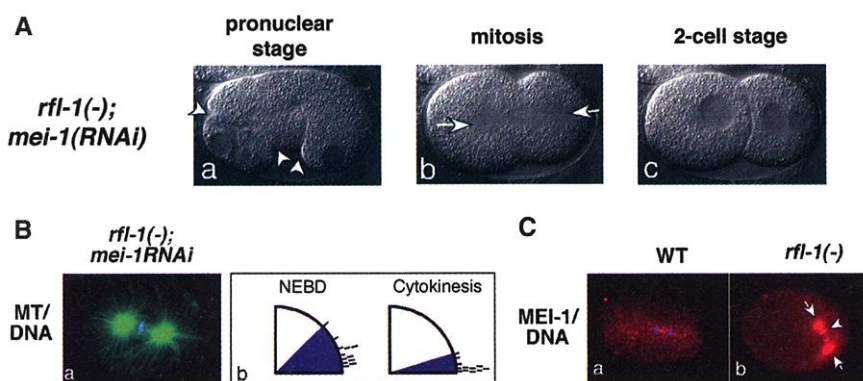


**Fig. 4.** (A) Nomarski micrographs of embryos from *rfl-1(or198ts)* hermaphrodites micro-injected with *mei-1* and *rfl-1* dsRNAs. Ectopic furrowing at the pronuclear migration stage still appeared (a, arrowheads), but spindle orientation and nuclear positioning defects, and ectopic cortical contractility during and after mitosis, were reduced or absent (b and c). (B) Confocal micrographs of  $\alpha$ -tubulin and DNA, in fixed *mei-1(RNAi)*; *rfl-1(or198tsRNAi)* embryo using indirect immunofluorescence. Most astral microtubules reach the cortex (a). Spindle orientation in multiple one-cell *mei-1(RNAi)*; *rfl-1(or198tsRNAi)* embryos (b), at nuclear envelope breakdown (NEBD) and during cytokinesis. (C) Confocal micrographs of MEI-1 and DNA in fixed one-cell embryos, using indirect immunofluorescence. MEI-1 was not detectable during mitosis in wild type (a) but was readily detected during mitosis in *rfl-1(or198ts)* mutant embryos at centrosomes (b, arrows) and on condensed DNA (b, arrowhead).

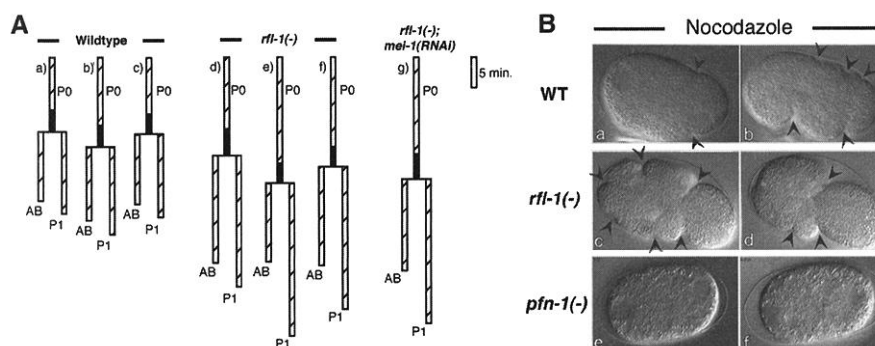


**Fig. 5.** (A) Cell-cycle timing. Vertical hatched bars and black bars indicate time spent during interphase and mitosis, respectively. Horizontal bars mark the completion of cell division. In a, b, d and e, timing is shown for individual embryos; in c and f, the average for 10 embryos is shown. Reducing *mei-1* function did not rescue the *rfl-1* cell-cycle delay ( $n = 5$  embryos). (B) Nomarski micrographs of embryos treated with nocodazole to disrupt microtubules. Wild-type embryos made roughly normal pseudocleavage furrows (a, arrowheads), and *rfl-1(or198tsRNAi)* mutants still exhibited extensive furrowing (c, arrowheads). Nocodazole treatment during mitosis resulted in extensive cortical contractility, in wild-type and *rfl-1(or198tsRNAi)* embryos (b and d, arrowheads). Inactivation of the contractile ring component *pfn-1* abolished all furrowing (e and f).